2022
9(1), 74-78

Journal of
MATERIALS NANOSCIENCE

Gas sensing of partially oxidized $Ti_3C_2T_x$ MXene in an argon atmosphere

Nasima Khatun,[1] Sanju Rani,[2] Govinda C Behera,[1] Somnath C Roy[1*]

[1]*Semiconducting Oxide Materials, Nanostructures, and Tailored Heterojunction (SOMNaTH) Lab, Department of Physics and 2D Materials and Innovation Group, Indian Institute of Technology Madras, Chennai, Tamil Nadu - 600036, India.* [2]*Department of Physics, SRMIST, Ramapuram Campus - 600089, Tamil Nadu, India*

Submitted on: 25-Nov-2021, Accepted and Published on: 15-Feb-2022

Article

ABSTRACT

Multilayer accordion-like $Ti_3C_2T_x$ MXene is prepared by selective etching of the Al layer from the Ti_3AlC_2 MAX phase. For better gas sensing responses, a minimal amount of TiO_2 decoration is being carried out by annealing the $Ti_3C_2T_x$ MXene in an argon atmosphere at 550 °C for 6 h. The X-ray diffraction pattern shows successful removal of Al layer and TiO_2 decoration on $Ti_3C_2T_x$ MXene surface which is well supported by field emission scanning electron microscope images. Due to TiO_2 decoration, MXene shows semiconducting behavior, and the corresponding bandgap is ~3.2 eV. TiO_2 decorated MXene sample shows the negative responses in presence of CH_4, H_2, and NO_2 gases at 100 °C. The sample shows a better response for NO_2, which is ~77 and ~12 times higher at 50 ppm compared to that of CH_4 and H_2. At 100 °C, the sample can detect ~5 ppm of NO_2 gas, which shows low-temperature sensor responses compared to that of conventional metal oxide semiconductor (200- 400 °C) sensors.

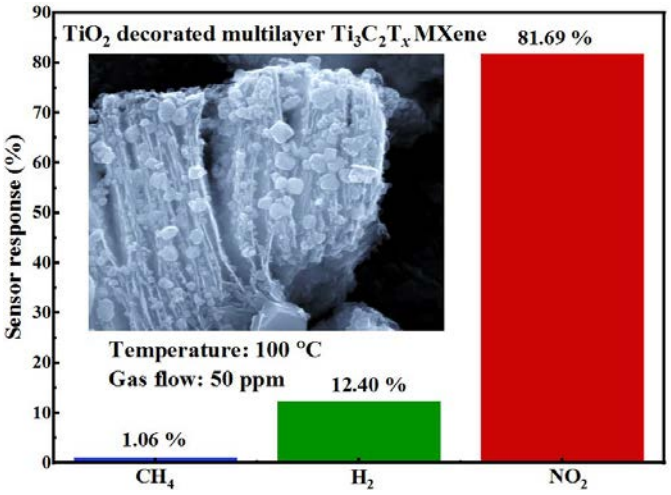

Keywords: $Ti_3C_2T_x$ MXene, Oxidation, TiO_2, Gas sensing, NO_2 selective

INTRODUCTION

Due to the modernization of society and industrial growth, the environment is being polluted by combustible, flammable, and toxic gases.[1-3] Hence, there is an urgent need to accurately monitor the levels of gases in the ambiance to ensure good health and safety of the living world. Gas sensors have the capabilities to detect the gases and quantify their concentrations.[4] Depending on working principle, different types of sensors are available, which include an electrochemical sensor, infrared sensor, ultrasonic sensor, and chemiresistive sensor. Among these, chemiresistive sensors are widely used because of portability, low cost, and long-term stability.[5] In chemiresistive sensors, a change in electrical resistance happens due to chemical reactions, when target gases are adsorbed on the surface of the sensing material.[6] Semiconductor metal oxides (TiO_2, SnO_2, In_2O_3, ZnO, CuO, etc.[7-9]) have been extensively used as a chemiresistive sensor, but they suffer from some critical problems such as high operating temperature (200-400 °C),[7,10] low electrical conductivity, and limited selectivity.[11] Hence, to resolve these problems, novel materials such as two-dimensional (2D) systems are being explored. The 2D materials have a very high surface area to volume ratio that provides more reactive sites for effective adsorption of target gas molecules and has a strong ability to transduce the interaction to an electrical signal.[12,13] Further, the surfaces can be functionalized with a variety of chemical groups to enhance selectivity towards a specific target gas. From the design perspective, 2D materials can easily be integrated with planer electronic devices which leads to their use as promising high-sensitive gas sensors.[14]

Among the recently discovered 2D materials, transition metal carbides and carbon nitrides called MXenes are gaining immense interest in almost every field including in gas sensor devices.[15] MXene is derived from *MAX* phase (*M* denotes early transition materials such as Ti, Sc, Hf; *A* denotes group III A or IV A elements, and *X* denotes carbon, nitrogen, or carbon and nitrogen together) materials by selective removal of strongly bonded *A* layers.[16-18] The chemical formula of MXene is $M_{n+1}X_nT_x$ (n = 1, 2, 3, …), where T_x denotes the surface terminated functional

*Corresponding Author: Dr. Somnath Chanda Roy, Professor, Department of Physics, HSB 119B, Indian Institute of Technology Madras, Chennai 600036 India
Tel: +91-44-2257-4886
Email : drsomnath@gmail.com, somnath@iitm.ac.in

URN:NBN:sciencein.jmns.2022.v9.308

ISSN: 2394-0867
https://pubs.thesciencein.org/jmns

groups such as -F, -O, and –OH.[19] The functional groups are randomly attached to the surface at the time of synthesis and its concentration/ratio can be controlled by changing the synthesis procedure.[20] MXenes also have high electrical conductivity and show strong hydrophilicity due to the surface terminated functional groups.[21,22] This unique combination makes them suitable for highly sensitive gas sensors. The high coverage of functional groups allows strong binding with analytes, whereas high metallic conductivity leads to a low noise.[13] Among the 2D MXenes, $Ti_3C_2T_x$ has been explored both theoretically and experimentally for gas sensing applications.[15] It is mainly used for volatile organic compounds (VOCs) such as acetone, ethanol, methanol, isopropanol, etc.[13,15,23] However, it is yet to be explored for combustible, flammable, and toxic gases. To make the MXene materials sensitive to these gases, different types of strategies such as hydrothermally treatment, composite formation, annealing the materials at different temperatures and atmospheres have been adopted.[20,24-26] In this work, we have treated the MXene in argon atmosphere so that it can be partially converted to semiconducting TiO_2 nanoparticles which is a very good chemiresistive sensor. The partial decoration of TiO_2 nanoparticles helps to detect the aforementioned gases and we observe a good response behavior at low temperature ~100 C° for NO_2 gas as compared to that of well-known metal oxide semiconductor sensor.

Experimental

1 gm of Titanium Aluminum Carbide (Ti_3AlC_2) was added to 20 ml of HF solution (48%) with continuous stirring at room temperature for 10 minutes to avoid overheating due to exothermic reaction. Stirring was continued for 24 h and then the mixture was washed with DI water several times through a centrifugation and decantation process until the *pH* reached ~ 6-7. The collected sediment was washed with isopropyl alcohol 2 times and dried overnight at room temperature in a vacuum chamber. The sample was denoted as $Ti_3C_2T_x$ -24. Thereafter the $Ti_3C_2T_x$ -24 sample was heated at 550 °C for 6 h in an argon atmosphere and named as $Ti_3C_2T_x$ -24 - 550.

Characterization

The crystallinity of the samples was characterized by an X-ray diffractometer (Bruker D8 Discover AXS) using CuK$_\alpha$ (1.54 Å) radiation in 2θ range 8 to 45°. Morphology and elemental compositions of the samples are analyzed by field emission scanning electron microscope (FESEM; FEI Inspect F50) attached with an energy dispersive X-Ray (EDX) detector. The bandgap of the samples is measured using diffuse reflectance spectroscopy carried out by Perkin Elmer LAMBDA 950 UV-VIS-NIR spectrophotometer. Fourier Transform Infrared Spectroscopy (FTIR) analysis was done by a BRUKER RFS system.

To make the devices for gas sensing measurement, 20 mg of the annealed powder was taken and mixed with 20 μL of Nafion solution and 0.5 mL of anhydrous ethanol and ultrasonicated for about ~30 minutes. The slurry was deposited on an aluminum substrate connected with a screen-printed, interdigitated patterned gold electrode (dropsens).

Results and Discussion

Figure 1 shows the XRD patterns of Ti_3AlC_2, $Ti_3C_2T_x$ - 24, and $Ti_3C_2T_x$ - 24 - 550 samples in 2θ range from 8 to 45 ° with a step size of 0.02°. The (002), (004), (101), (103), and (104) peaks correspond to the MAX phase of Ti_3AlC_2.[27] However, there is a small presence of TiC compounds corresponding to (111) and (200) peaks at 36.0° and 41.7°, which remain as residue of precursor [28]. After 24 h HF etching, the main peak (104) at ~38.8 ° disappears completely and on the same time (002) and (004) peaks broaden and shifted to lower 2θ values, which indicates the removal of the Al layers and increase of the interplanar spacing [19] and confirms the synthesis of 2D $Ti_3C_2T_x$ MXene. (111) and (200) peaks of TiC remain because it is difficult to remove by HF etching [29,30]. Heating the $Ti_3C_2T_x$ - 24 sample in an argon atmosphere at 550 °C for 6 h with a ramp rate of 2.5 °C/min shows a TiO_2 (101) peak (25.32 °), which corresponds to the anatase phase.[31,32] When multilayer MXene are heated in the argon atmosphere the water molecules present in between the MXene layers react with the MXene surface and TiO_2 is formed on the surface. This is also observed by the reduced intensity of (002) peak, it happens as interlayer spacing reduces by the removal of water molecules.[14]

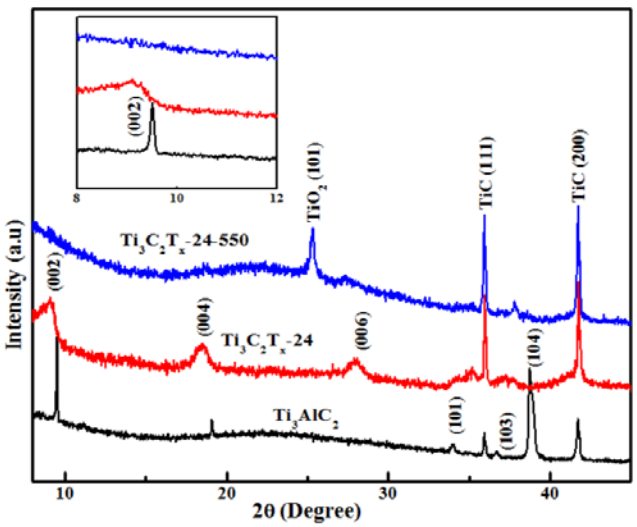

Figure 1. XRD pattern of Ti_3AlC_2, $Ti_3C_2T_x$ - 24, and $Ti_3C_2T_x$ - 24 - 550 samples respectively.

The morphology of the samples investigated through FESEM is shown in Figure 2. Figure 2(a) is the FESEM image of the Ti_3AlC_2 MAX phase which reveals a compact 3D layered structure. After 24 h HF etching, Al layers are removed, and it becomes an accordion-like multilayer 2D $Ti_3C_2T_x$ MXene. EDX shows Al presence in Ti_3AlC_2 is ~ 9.7% (Figure (2 (d))), while after HF etching it becomes ~1.7% (Figure (2 (e))), which signifies Al layers are removed and multilayer $Ti_3C_2T_x$ MXene is synthesized successfully, which is well supported by XRD results. EDX also shows that O and F elements are present in multilayer $Ti_3C_2T_x$ MXene and are attached to the surface as functional groups during the synthesis process.[16] FESEM image of $Ti_3C_2T_x$ - 24 - 550 sample (Figure 2(c)) shows smaller particles

on the surface of $Ti_3C_2T_x$ MXene, which are TiO_2, and it is formed due to annealing in an argon atmosphere. The oxygen of water molecules presents in between the layers react with Ti of $Ti_3C_2T_x$ MXene and due to oxidation, some portion of MXene is converted into TiO_2.

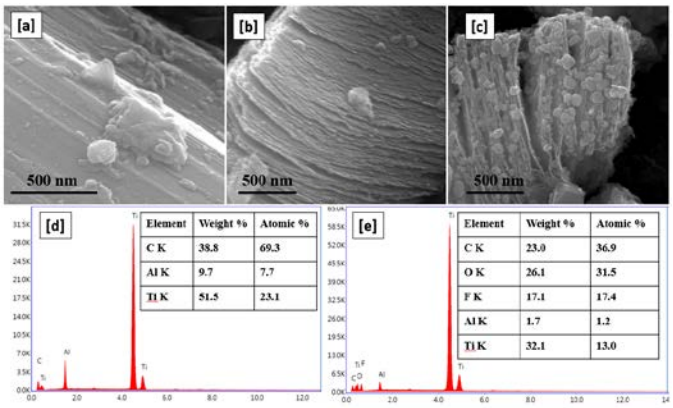

Figure 2 (a, b, and c) FESEM images of Ti_3AlC_2, $Ti_3C_2T_x$ - 24, and $Ti_3C_2T_x$ - 24 - 550 samples respectively, and (d, and e) EDX of Ti_3AlC_2 and $Ti_3C_2T_x$ - 24 samples.

The Tauc plots obtained from the diffuse reflectance spectroscopy (DRS) data of Ti_3AlC_2, and $Ti_3C_2T_x$ - 24 samples (Figure 3(a)) show metallic behavior, which is well supported with reported value.[33] The metallic behavior is characterized by reasonably high reflectance in the entire range of wavelengths. This originates from the higher conductivity of the MXene samples. Annealing at argon atmosphere results in TiO_2 decoration on the surface of MXene which leads to the semiconducting nature of partially oxidized MXene ($Ti_3C_2T_x$ - 24 - 550) and bandgap become ~3.20 eV. This is evident by the absorption edge in the Tauc plot and close to the reported values.[34,35]

Figure 3 (b) shows the FTIR spectra of Ti_3AlC_2, $Ti_3C_2T_x$ - 24, and $Ti_3C_2T_x$ - 24 - 550 samples respectively. For all the samples the vibration in between 500 - 680 cm^{-1} arises due to Ti-C stretching vibration denotes a very minute change in the internal atomic structure of Ti_3C_2 layers even after HF etching and annealing the sample at 550 °C.[36,37] The evidence of surface terminated functional groups (-O, -F, and -OH) in MXene are observed by the vibration in the range ~910-1180 cm^{-1} and ~145–1330 cm^{-1} corresponds to C-O and C-F stretching vibration and the vibration from 1380 cm^{-1} to higher wavenumber corresponds to -O-H bending bands [36,38,39]. The vibration at ~590 cm^{-1} corresponds to Ti-O stretching vibration due to the formation of TiO_2 particles on the edge and surface of $Ti_3C_2T_x$ MXene.[40]

Gas sensing experiments are performed in a sealed chamber fitted with X-Y-Z manipulators, sample heating stage, electrical probes, and gas injection and ejection ports as shown in Figure 4. The amount of gas injected into the chamber was controlled by using Mass Flow Controllers and the concentration was further reduced by mixing with zero air. The experiment is carried out at 100 °C. The gas sensing characteristics were quantified by measuring the change in resistance to gas exposure with respect to carrier gas (zero air).

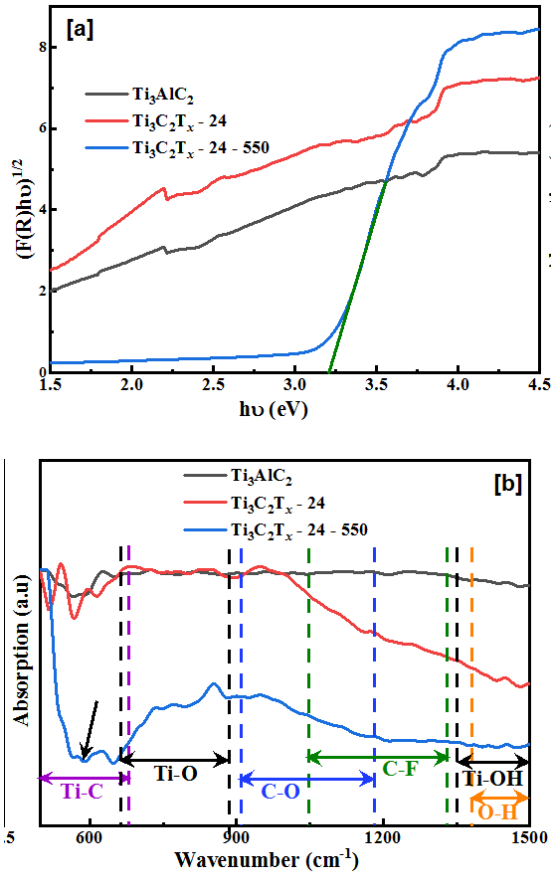

Figure 3. (a) Tauc plot of DRS data and (b) FTIR of Ti_3AlC_2, $Ti_3C_2T_x$ - 24, and $Ti_3C_2T_x$ - 24 - 550 samples respectively.

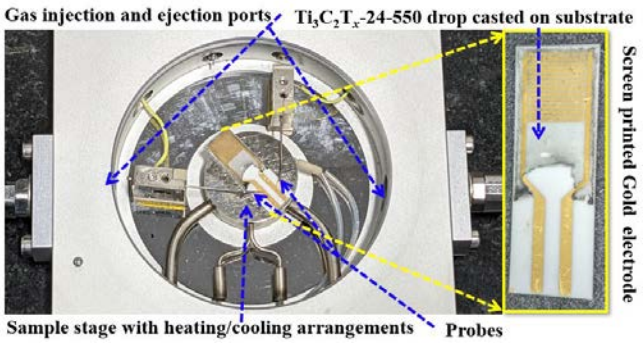

Figure 4. Gas sensing chamber fitted with sample heating stage, electrical probes, and gas injection and ejection ports**.**

Figure 5(a) shows the gas sensing curves of $Ti_3C_2T_x$ - 24 - 550 sample for 50 ppm of the target gases such as methane (CH_4), hydrogen (H_2), and nitrogen dioxide (NO_2). The sample shows a decrease in resistance for all the gases (CH_4, and NO_2) irrespective of their reducing (CH_4 and H_2) and oxidizing (NO_2) nature. Response /recovery time (time taken to change the resistance ~90%) and sensor response (R) is calculated by $(R_g-R_a)/R_a$, where R_g is the resistance in presence of gas and R_a is the resistance in presence of air.

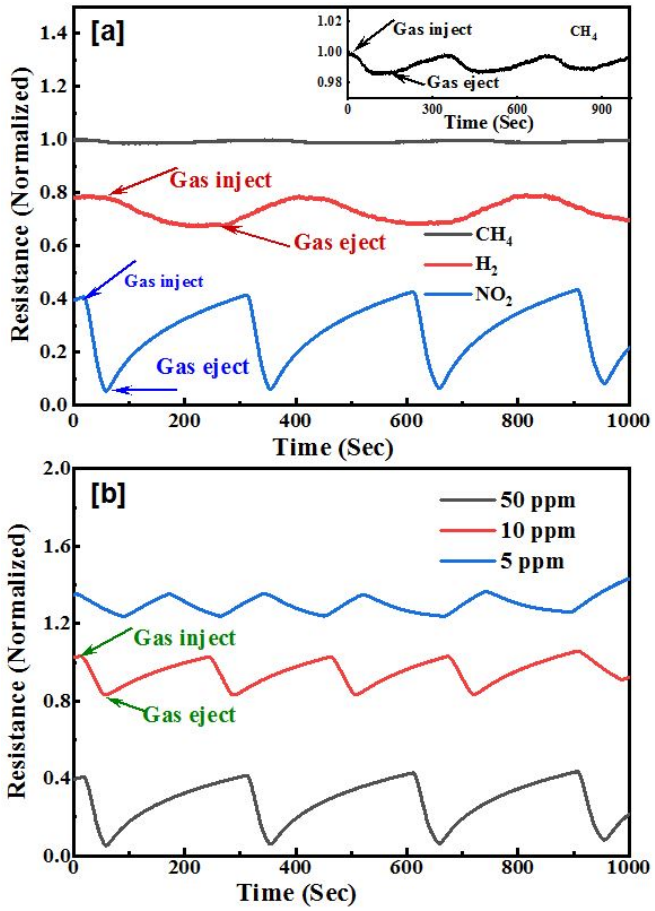

Figure 5. (a) Gas sensing (change in resistance (normalized)vs time (Sec)) curves for $Ti_3C_2T_x$ - 24 – 550 samples at 100 °C for CH_4, H_2, and NO_2 gases, Figure5 (b) Gas sensing (change in resistance (normalized)vs time (Sec)) curves for $Ti_3C_2T_x$ - 24 - 550 samples at 100 °C for different concentration of NO_2 gas.

Table 1: Response time, recovery time, and sensor responses for 50 ppm at 100 °C for CH_4, H_2, and NO_2.

S.No	Gases	Response time (Sec)	Recovery time (Sec)	Sensor response (%)
1	CH_4	57.48	119.27	1.06
2	H_2	111.77	98.63	12.40
3	NO_2	31.17	185.03	81.69

Table 2: Response time, recovery time, and sensor responses for $Ti_3C_2T_x$ - 24 - 550 sample at 100 °C for different concentrations of NO_2 gas.

S.No	NO_2 (ppm)	Response time (Sec)	Recovery time (Sec)	Sensor response (%)
1	50	31.17	185.03	81.69
2	10	32.83	142.78	26.65
3	5	81.20	61.18	14.69

Though for all gases, the sample shows negative responses, the sensor response is better in the case of NO_2 (Table 1), which is ~77 and ~12 times higher compared to that of CH_4 and H_2 gases. Hence, we have performed sensing responses for a lower concentration of NO_2 gas (10 ppm and 5 ppm) (Table 2). It is observed that even for 5ppm of NO_2, the sample has a higher response compared to that of CH_4 and H_2 at 50 ppm.

In general, the hydrogen atom-containing gases such as CH_4 and H_2 are considered reducing in nature as they donate electrons to the interacting surface; whereas NO_2 is an oxidizing gas, which withdraws electrons. From the Tauc plot, it is observed that the $Ti_3C_2T_x$ - 24 - 550 becomes semiconductor (3.20 eV) due to the presence of TiO_2 decoration on the surface of multilayer $Ti_3C_2T_x$ MXene. In most cases, the TiO_2 decorated MXene sample behaves like an n-type semiconductor,[14] but here in our case annealing at argon atmosphere shows p-type semiconductor behavior. From literature, it is observed that Ti vacancies are responsible for p-type conductivity for TiO_2,[41] here TiO_2 formed on MXene surfaces in argon atmosphere may contain Ti vacancies, which is responsible for the p-type behavior of the sample for NO_2 gas. However, for CH_4 and H_2, it behaves n-type. We know that pristine MXene has metallic conductivity. Hence, a detailed fundamental study is required to explain such an anomalous sensing behavior of argon atmosphere annealed multilayer MXene sample.

Conclusion

A minimal amount of TiO_2 decoration on $Ti_3C_2T_x$ MXene is fabricated by annealing the multilayer MXene at 550 °C in an inert atmosphere. FESEM image shows smaller nanoparticles are present on MXene surfaces and the XRD pattern shows that the nanoparticles correspond to the TiO_2 anatase phase. The TiO_2 decoration is also supported by EDX and FTIR results. From the Tauc plot, it is observed that the bandgap of the TiO_2 decorated MXene sample is ~3.2 eV. At 100 °C temperature, the sample shows negative responses for all the gases (CH_4, H_2, and NO_2 for 50 ppm). For 50 ppm of NO_2 gas, the sample shows ~77 and ~12 times higher response compared to that of CH_4 and H_2. For our sample at 100 °C, NO_2 can be detected even for a lower (5 ppm) concentration which is a very good sensor behavior compared to the other conventional metal oxide semiconductors (200-400 °C).

Acknowledgment

Nasima Khatun acknowledges the IIT Madras Institute's postdoctoral fellowship scheme for financial support and all research-related facilities. Authors thanks the central facilities of the MME department for providing the XRD facility. The authors also acknowledge the Sophisticated Analytical Instrument Facility (SAIF) of IIT Madras for providing UV-vis spectroscopy, and FTIR facilities.

Conflict of Interest

Authors declared no conflict of interest.

References

1. Z. Zhu, S.-J. Lin, C.-H. Wu, R.-J. Wu. Synthesis of TiO_2 nanowires for rapid NO_2 detection. *Sens. Actuator A: Phys.* **2018**, 272288-94.
2. B. Comert, N. Akin, M. Donmez *et. al.* Titanium dioxide thin films as methane Gas Sensors. *IEEE Sens. J.* **2016**, 16(24), 8890-96.

3. Z. Li, Z. Yao, A.A. Haidry *et. al.* Resistive-type hydrogen gas sensor based on TiO_2: A review. *Int. J. Hydrog. Energy* **2018**, 43(45), 21114-32.
4. Q. Sun, J. Wang, X. Wang *et. al.* Treatment-dependent surface chemistry and gas sensing behavior of the thinnest member of titanium carbide MXenes. *Nanoscale* **2020**.
5. Z. Meng, R.M. Stolz, L. Mendecki, K.A. Mirica. Electrically-transduced chemical sensors based on two-dimensional nanomaterials. *Chemical reviews* **2019**, 119(1), 478-598.
6. L. Pirondini, E. Dalcanale. Molecular recognition at the gas-solid interface: a powerful tool for chemical sensing. *Chem Soc Rev* **2007**, 36(5), 695-706.
7. S. Ng, J. Prasek, R. Zazpe *et. al.* Atomic layer deposition of SnO_2-Coated anodic one-dimensional TiO_2 nanotube layers for low concentration NO_2 sensing. *ACS Appl. Mater. Interfaces* **2020**, 12(29), 33386-96.
8. S.B. Kondawar, A.M. More, H.J. Sharma, S.P. Dongre. Ag-SnO2/Polyaniline composite nanofibers for low operating temperature hydrogen gas sensor. *J. Mater. Nanosci.* **2017**, 4 (1), 13–18.
9. V.S. Bhati, M. Hojamberdiev, M. Kumar. Enhanced sensing performance of ZnO nanostructures-based gas sensors: A review. *Energy Reports* **2020**, 646-62.
10. S. Zou, J. Gao, L. Liu *et. al.* Enhanced gas sensing properties at low working temperature of iron molybdate/MXene composite. *J. Alloys Compd.* **2020**, 817152785.
11. Z. Zhu, C. Liu, F. Jiang *et. al.* Flexible and lightweight $Ti_3C_2T_x$ MXene@Pd colloidal nanoclusters paper film as novel H_2 sensor. *Journal of hazardous materials* **2020**, 399123054.
12. X. Liu, T. Ma, N. Pinna, J. Zhang. Two-dimensional nanostructured materials for gas sensing. *Adv. Funct. Mater.* **2017**, 27(37), 1702168.
13. S.J. Kim, H.J. Koh, C.E. Ren *et. al.* Metallic $Ti_3C_2T_x$ MXene gas sensors with ultrahigh signal-to-noise ratio. *ACS Nano* **2018**, 12(2), 986-93.
14. H. Pazniak, I.A. Plugin, M.J. Loes *et. al.* Partially oxidized $Ti_3C_2T_x$ MXenes for fast and selective detection of organic vapors at part-per-million concentrations. *ACS Appl. Energy Mater.* **2020**, 3(4), 3195-204.
15. E. Lee, D.-J. Kim. Review- Recent exploration of two-dimensional MXenes for gas sensing: From a theoretical to an experimental view. *J. Electrochem. Soc.* **2020**, 167(3), 037515.
16. M. Naguib, M. Kurtoglu, V. Presser *et. al.* Two-dimensional nanocrystals produced by exfoliation of Ti_3AlC_2. *Adv. Mater.* **2011**, 23(37), 4248-53.
17. M. Khazaei, A. Ranjbar, M. Arai *et. al.* Electronic properties and applications of MXenes: A theoretical review. *J. Mater. Chem. C* **2017**, 5(10), 2488-503.
18. Y. Xie, P.R.C. Kent. Hybrid density functional study of structural and electronic properties of functionalized $Ti_{n+1}X_n$(X=C, N) monolayers. *Phys. Rev. B* **2013**, 87(23).
19. V.M. Hong Ng, H. Huang, K. Zhou *et. al.* Recent progress in layered transition metal carbides and/or nitrides (MXenes) and their composites: synthesis and applications. *J. Mater. Chem. A* **2017**, 5(7), 3039-68.
20. M. Wu, M. He, Q. Hu *et. al.* Ti_3C_2 MXene-based sensors with high selectivity for NH_3 detection at room temperature. *ACS Sens* **2019**, 4(10), 2763-70.
21. J. Zhang, N. Kong, S. Uzun *et. al.* Scalable manufacturing of free-standing, strong $Ti_3C_2T_x$ MXene films with outstanding conductivity. *Adv. Mater.* **2020**, 32(23), e2001093.
22. H. Wang, Y. Wu, X. Yuan *et. al.* Clay-inspired MXene-based electrochemical devices and photo-electrocatalyst: State-of-the-art progresses and challenges. *Adv. Mater.* **2018**, 30(12), e1704561.
23. W. Yuan, K. Yang, H. Peng *et. al.* A flexible VOCs sensor based on a 3D Mxene framework with a high sensing performance. *J. Mater. Chem. A* **2018**, 6(37), 18116-24.
24. S. Liu, M. Wang, G. Liu *et. al.* Enhanced NO_2 gas-sensing performance of 2D Ti_3C_2/TiO_2 nanocomposites by in-situ formation of Schottky barrier. *Appl. Surf. Sci.* **2021**, 567150747.
25. J. Choi, Y.J. Kim, S.Y. Cho *et. al.* In situ formation of multiple Schottky barriers in a Ti_3C_2 MXene film and its application in highly sensitive gas sensors. *Adv. Funct. Mater.* **2020**, 30(40), 2003998.
26. S.H. Lee, W. Eom, H. Shin *et. al.* Room-temperature, Highly durable $Ti_3C_2T_x$ MXene/Graphene hybrid fibers for NH_3 gas sensing. *ACS Appl. Mater. Interfaces* **2020**, 12(9), 10434-42.
27. N. Khatun, S. Dey, G.C. Behera, S.C. Roy. $Ti_3C_2T_x$ MXene functionalization induced enhancement of photoelectrochemical performance of TiO_2 nanotube arrays. *Mater. Chem. Phys.* **2022**, 278125651.
28. B. Scheibe, V. Kupka, B. Peplinska *et. al.* The Influence of oxygen concentration during MAX phases (Ti_3AlC_2) preparation on the alpha-Al_2O_3 microparticles content and specific surface area of multilayered MXenes ($Ti_3C_2T_x$). *Mater.* **2019**, 12(3).
29. Z. Guo, L. Gao, Z. Xu *et. al.* High electrical conductivity 2D MXene serves as additive of perovskite for efficient solar cells. *Small* **2018**, 14(47), e1802738.
30. O. Mashtalir, M. Naguib, V.N. Mochalin *et. al.* Intercalation and delamination of layered carbides and carbonitrides. *Nat. Commun.* **2013**, 41716.
31. N. Khatun, S. Tiwari, R. Amin *et. al.* Stable anatase phase with a bandgap in visible light region by a charge compensated Ga–V (1:1) co-doping in TiO_2. *Ceram. Int.* **2020**, 46(7), 8958-70.
32. N. Khatun, S. Dey, T. Appadurai *et. al.* Enhanced H_2 evolution through water splitting using TiO_2/ultrathin g-C_3N_4: A type II heterojunction photocatalyst fabricated by in situ thermal exfoliation. *Appl. Phys. Lett.* **2021**, 119(9), 093901.
33. M. Khazaei, M. Arai, T. Sasaki *et. al.* Novel electronic and magnetic properties of two-dimensional transition metal carbides and nitrides. *Adv. Funct. Mater.* **2013**, 23(17), 2185-92.
34. N. Khatun, S. Tiwari, J. Lal *et. al.* Stabilization of anatase phase by uncompensated Ga-V co-doping in TiO_2: A structural phase transition, grain growth and optical property study. *Ceram. Int.* **2018**, 44(18), 22445-55.
35. N. Khatun, Anita, R. Amin, S. Sen. Bandgap tuning by lattice distortion in V and Ga doped TiO_2. *Integr. Ferroelectr. Integr.* **2019**, 194(1), 91-95.
36. Z. Wang, J. Xuan, Z. Zhao *et. al.* Versatile cutting method for producing fluorescent ultrasmall MXene sheets. *ACS Nano* **2017**, 11(11), 11559-65.
37. A. Sengupta, B.V.B. Rao, N. Sharma *et. al.* Comparative evaluation of MAX, MXene, NanoMAX, and NanoMAX-derived-MXene for microwave absorption and Li ion battery anode applications. *Nanoscale* **2020**, 12(15), 8466-76.
38. E. Satheeshkumar, T. Makaryan, A. Melikyan *et. al.* One-step solution processing of Ag, Au and Pd@MXene hybrids for SERS. *Sci. Rep.* **2016**, 632049.
39. Y. Sun, Z. Xu, Y. Zhuang *et. al.* Tunable dextran retention of MXene-TiO_2 mesoporous membranes by adjusting the 2D MXene content. *2D Materials* **2018**, 5(4), 045003.
40. G. Rajakumar, A.A. Rahuman, S.M. Roopan *et. al.* Fungus-mediated biosynthesis and characterization of TiO_2 nanoparticles and their activity against pathogenic bacteria. *Spectrochim. Acta A: Mol. Biomol. Spectrosc.* **2012**, 9123-9.
41. S. Wang, L. Pan, J.J. Song *et. al.* Titanium-defected undoped anatase TiO_2 with p-type conductivity, room-temperature ferromagnetism, and remarkable photocatalytic performance. *J. Am. Chem. Soc.* **2015**, 137(8), 2975-83.